## Automated Pneumonia Detection from Chest X-ray Images Using Optimized Feature Selection and Artificial Intelligence

# Sheela T<sup>1</sup>, Nagendra Nath Giri<sup>1</sup>, Santhosh Kumar B N<sup>2</sup>, Prakasha Raje Urs M<sup>2</sup>

<sup>1</sup>Associate Professor, Department of Computer Science, Maharani's Science College for Women (Autonomous), Mysuru, Karnataka 570005, India <sup>2</sup>Assistant Professor, Department of Computer Science, Maharani's Science College for Women (Autonomous), Mysuru, Karnataka 570005, India

Pneumonia is one of the primary causes of death in both children and older people, affecting around 4 million lives every year. It may be triggered by viruses, bacteria, or fungi, depending on the pathogen that infects the lung's small air sacs. Patients with underlying conditions such as asthma, weakened immunity, hospitalized infants, and the elderly on ventilation systems are at greater risk if pneumonia is not recognized early. Although many existing diagnostic approaches are available, limited accuracy and efficiency require further research. This study employs optimized feature selection and Artificial Intelligence (AI) techniques to improve the accuracy of automated pneumonia detection. Chest X-ray (CXR) images are used as data. The dataset is preprocessed to make it suitable for pneumonia classification. Three types of features are extracted from the CXR images using the Histogram of Oriented Gradients (HOG), Gray-Level Co-occurrence Matrix (GLCM), and Local Binary Patterns (LBP) algorithms. Additionally, two more features are created using fusion techniques and the Grasshopper Optimization Algorithm (GOA). All five features are fed into the AI model. The Naive Bayes (NB) algorithm is used as the AI model. The NB model's performance is evaluated using various performance measures. Experimental outcomes show that the NB model with optimized features achieved the highest accuracy score of 98.33% and the lowest False Rejection Rate (FRR) and False Acceptance Rate (FAR) of 1.69% and 1.64%, respectively. The model's performance in pneumonia identification indicates that the proposed method (GOA+NB) could efficiently categorize normal and pneumonia X-rays, thereby relieving the workload of radiologists.

**Keywords:** Pneumonia, Chest X-Ray, Feature Extraction, Grasshopper Optimization, Naïve Bayes, Positive Metrics.

### 1. Introduction

Pneumonia is a common infectious disease usually caused by bacterial or viral infections [1]. Pneumonia is extremely serious and may cause death if not treated promptly [2]. As a result,

early detection is critical for properly diagnosing and treating pneumonia. The rapid film creation and inexpensive cost of CXR images make them excellent for diagnosing pneumonia [3]. Currently, having a doctor or expert sit down in a clinic and manually identify pneumonia from X-ray images is the standard procedure. This strategy is less cost-effective, heavily reliant on the diagnosing physician's clinical experience, and prone to huge accuracy swings [4]. In less developed areas, a lack of competent medical experts and specialized technology makes it difficult to diagnose pneumonia quickly. As a result, pneumonia has a high death rate in developing countries and regions, wreaking havoc on people's lives and health.

The use of computer-aided pneumonia diagnostic tools has improved the efficiency and accuracy of pneumonia detection. Recent breakthroughs in AI have resulted in its extensive application in healthcare, particularly in the identification of pneumonia. AI's excellent accuracy and robustness have greatly improved the efficiency of pneumonia diagnosis.

Many academics have investigated AI's abilities in pneumonia detection. The study [5] assessed the three textural image characterization techniques for their potential as biomarkers for developing AI models to identify pneumonia in computed tomography images. The models of three AI techniques have been examined. This study used two publicly available image datasets. The findings support the claimed methods' reliability and user-friendliness as automated pneumonia diagnosis devices. The goal of the study [6] was to identify COVID-19 in CXR images using five different AI models. The research aims to examine CXR images using specific AI models. To be more specific, ResNet101, DenseNet169, ResNet50, DenseNet121, and InceptionV3 models are provided. All models have been trained and verified on a large openly accessible collection of COVID-19 CXR dataset. Furthermore, their usefulness and utility in a medical setting were proven through reviews of previously discovered data. Even though ResNet101 was the top model, they all performed well.

In research [7], a viable technique is presented for recognizing COVID-19 from CXR and computed tomography images using AI methods. The core classification mechanism is based on EfficientNet and MixNet, two recently discovered deep neural network (DNN) families. The three different transfer learning (TL) methods are employed to enhance the training process. The ultimate objective is to develop an AI diagnostic system capable of accurately detecting COVID-19 from various images. The proposed method was evaluated on four realworld datasets. To evaluate the method, the 5-fold cross-validation technique was employed. For each dataset considered, the model achieves promising prediction performance. The achieved accuracy is consistently more than 95.0% across all configurations. The paper [8] thoroughly examines an advanced technique for pneumonia identification utilizing the Vision Transformer (ViT) framework using a publicly available CXR dataset from Kaggle. The recommended approach uses the ViT network, which blends the self-attention module with the transformer structure, to extract global and spatial relationships from CXR images. The study discovered that the proposed Vision Transformer-based system outperformed the current methods in CXR pneumonia identification. The ViT model is ideal for better understanding spatial relationships, capturing global context, and interpreting images of varied resolutions.

The article [9] describes a technique that uses adversarial training and TL to increase the accuracy of CXR pneumonia diagnosis. To accomplish this, the authors pre-train the AlexNet architecture on the huge ImageNet dataset before applying it to retrieve the valuable features

from the CXR dataset. Then the network is trained to detect pneumonia on a subset of annotated X-rays. To deal with sparsely labelled data, the authors use an adversarial training technique. This method involves training an extra network to produce synthetic X-rays that closely mimic real X-rays but have minor differences. They improved the detection network's generalizability and durability by training it on both synthetic and real X-rays. When compared to previous approaches, the scientists discovered that their methodology produces significantly higher accuracy on a publicly available pneumonia dataset. In addition, they demonstrate that their adversarial training strategy increases the network's generalizability to new X-rays while decreasing the chance of over-fitting.

In the paper [10], a hybrid AI design is recommended for detecting pneumonia in CXR images. Before employing Long Short Term Memory, the images are enhanced with an Adaptive Median Filter. A regularized DNN is then employed for retrieving the features. The last phase involves using the attention strategy to guide the network's attention to the suitable features. The proposed method was evaluated on two openly accessible CXR datasets of pneumonia. As a last stage in the experiments, a color visualization technique is used based on Grad-CAM to appropriately interpret radiological images of pneumonia. The results were superior to those obtained using cutting-edge approaches. The aim of the study [11] is to utilize digital X-ray images to automate the differentiation of bacterial and viral pneumonia. SqueezeNet, AlexNet, ResNet18, and DenseNet201 are the four DNNs employed for TL. The classification task was trained by TL on a pre-processed collection of 5247 images, including CXR images of bacterial, viral, and normal states. The study's authors proposed three ways to classify pneumonia: identifying a mix of normal and viral cases, bacterial and viral infections individually, or a combination of the two. It outperforms previously reported accuracies.

In this research, we employed AI and optimization techniques to improve pneumonia detection from CXR images. The effectiveness of the proposed method is evaluated using positive and negative measures.

### 2. Background Study

To automate pneumonia detection, feature extraction, fusion, and selection techniques are used for retrieving the features, and an AI model is employed for classification. The working of feature extraction algorithms such as HOG, GLCM, and LBP, as well as feature selection algorithms like GOA and the NB classifier, are detailed in this section.

### A. Feature Extraction: HOG

According to a study [12], one of the most commonly utilized descriptor features in image processing is the HOG method. The HOG feature enhances the accuracy of the recognition process. The accuracy of the image is improved by using a module, which is its smallest gradient. The estimated gradient indicates that the HOG feature provides certain benefits in terms of direction invariance and intensity robustness [13]. The value of the local histogram is combined with the other cells in the assigned module to normalize the module's area intensity. This normalizing technique works well in both bright and low-light conditions. The vertical and horizontal gradient directions are calculated using the image's pixels and a certainty kernel factor. The horizontal gradient indicates the image's magnitude, while the vertical gradient

indicates its direction. Equation (1) represents how to calculate the magnitude's gradient |G|, which is determined by the vertical and horizontal pixel's intensity,  $I_x$  and  $I_y$ . Equations (2) and (3) are applied to calculate  $I_x$  and  $I_y$ . Alternatively, Equation (4) can be utilized to calculate the value of the direction image,  $\theta$ .

$$|G| = \sqrt{I_x^2 + I_y^2}$$
 [1]

$$I_x = I * D_x; D_x = [-1 \ 0 \ 1]$$
 [2]

$$I_v = I * D_v; D_v = [-1 \ 0 \ 1]$$
 [3]

$$\theta = \arctan\left(\frac{I_y}{I_x}\right) \tag{4}$$

To make a bin of the directions of the histogram, first partition the image's magnitude and direction components into specific modules. Next, HOG features are generated by the bin's layout.

### B. Feature Extraction: GLCM

Statistical second-order texture information can be extracted from gray-level images using features like GLCM, which are texture-based [14]. These features are focused on a specific location of the pixels in comparison to the other pixels because the image feature often offers vital information about the ordered arrangement of surfaces. GLCM has demonstrated its ability to generate strong outcomes in various domains, one of which is medical image diagnosis [15]. Energy, contrast, entropy, homogeneity, shade, and prominence were the seven textural features that were retrieved from CXR images using GLCM. The formula used to calculate the textural features is given in Equation (5-11).

Energy = 
$$\sqrt{\sum_{x=0}^{m-1} \sum_{y=0}^{m-1} \sum_{y=0}^{m-1} f^2(x,y)}$$
 [5]

Contrast = 
$$\sum_{x=0}^{m-1} \sum_{y=0}^{m-1} (x-y)^2 f(x,y)$$
 [6]

Entropy = 
$$-\sum_{x=0}^{m-1} \left[ \sum_{y=0}^{n-1} \left[ f(x,y) \log_2 f(x,y) \right] \right]$$

IDM = 
$$\sum_{x=0}^{m-1} \frac{1}{x} \sum_{y=0}^{m-1} \frac{1}{x} \frac{1}{1+(x-y)^2} f(x,y)$$
 [8]

$$SD = \sqrt{\left(\frac{1}{mxn}\right)\sum_{x=0}^{m-1} \left[ \sum_{y=0}^{m-1} \left[ f(x,y) - M^2 \right] \right]}$$
 [9]

Skewness = 
$$\left(\frac{1}{\text{mxn}}\right) \frac{\sum_{\square}^{\square} \square f(x,y) - M^3}{\partial^3}$$
 [10]

Correlation = 
$$\frac{\sum_{x=0}^{m-1} \square \sum_{y=0}^{n-1} \square (x,y) f(x,y) - M_x M_y}{\partial_x \partial_y}$$
 [11]

In the above equations, f(x, y) represents the pixel intensity, M represents the mean value, and  $\theta$  represents the standard deviation.

### C. Feature Extraction: LBP

Computer vision researchers have made extensive use of the LBP operator, a texture descriptor. Its ease of use, rapid computation, and tolerance to illumination fluctuations make it an excellent choice for defining local texture patterns [16]. The LBP operator computes differences between adjacent pixels to generate a local representation of textured images. An LBP is calculated for each image's spatial position by considering the surrounding pixels [17]. Finding the histogram of the LBP produces the feature vector. Taking circular neighbourhoods of diverse sizes into account allows the enhanced LBP variation to generate texture features at many scales. A multi-resolution technique can also be used to establish invariance in the observation scale. Combining feature vectors captured at various scales is a key component of the multi-resolution method. The generated features rotation invariance is improved by an additional homogeneity condition. A pattern is deemed uniform if it has no more than two bitwise transitions. The likelihood of the pattern shifting during rotation increases if there are many spatial transitions in it. With the homogeneity criterion in place, the feature vector is smaller and rotation invariance is improved [18]. Noise also produces a great deal of pattern transitions, which leads to oscillations either below or above the core pixel, because it is fundamentally unpredictable. The uniformity criterion prevents the noisy patterns instead of discarding them as non-uniform. The uniformity function, U, represents the number of transitions. To compute the uniform rotation-invariant LBP (riu2), the Equation (12) is used:

$$LBP_{RP}^{riu2}(x_c) = \{\sum_{n=0}^{P-1} | || s(x_c - x_{RP,n}), \text{ if } U(LBP_{RP}) \le 2 P + 1, \text{ otherwise } [12] \}$$

where  $x_c$  represents the central pixel, s(x) represents the sign function from Equation (13),  $x_{R,P,n}$  represents the  $n^{th}$  neighbour pixel from a neighbourhood with P neighbors and R is the radius, and U is the uniformity function.

$$s(x) = \{0, \text{ if } x < 0 \ 1, \text{ if } x \ge 0 \}$$
 [13]

There are exactly P+1 uniform patterns (UP) in a neighbourhood with P neighbors. All non-uniform patterns (NUP) are combined under the mixed label P+1, whereas UPs are labelled separately based on the total bits in the pattern. There are P+2 bins in the histogram that correspond to the LBP codes obtained. Since NUPs can be eliminated, the final feature vector is P+1 in size.

### D. Feature Fusion

Feature fusion involves two types namely early and late fusion [19]. During early fusion, many layers' features are fused before the predictor is trained on them. Late fusion involves making predictions before the ultimate fusion is completed, and in the end, several forecasts are fused. An early fusion approach is chosen since late fusion fails to address the underlying issue of inadequate feature information. Early fusion also makes use of several fusion techniques, such as Concat and Add. This study makes use of the Add fusion method, which enriches the image-describing vector of features along each dimension. Also, the dimensionality remains unchanged, and the Add technique requires significantly less processing than the Concat method. When the GLCM, HOG and LBP features are fused, a combined feature vector is generated. The Add fusion method's computations are based on the Equation (14):

$$Z_{add} = \sum_{i=1}^{c} \mathbb{III} (X_i + Y_i) * K_i$$
 [14]

Nanotechnology Perceptions Vol. 20 No. S13 (2024)

The weighted vector is denoted by  $K_i$ , the input channels are represented by  $X_i$  and  $Y_i$ , convolution is denoted by \*, and the fusion feature vector is denoted by  $Z_{add}$ . To attain feature complementarity, the primary goal of Add fusion is to combine the features obtained from all three algorithms.

### E. Feature Selection: GOA

Using the feature selection process, the most relevant features are selected to achieve the goal of accuracy improvement. The GOA was utilized for feature selection in this study. This strategy is intended to converge early in the feature selection step so that it can converge as much as possible in the final optimization stage [20]. The grasshopper is an insect that is considered a pest because it causes damage to crops and other agricultural items [21]. Equation (15) is utilized to model the activities of grasshoppers.

$$X_i = S_i + G_i + A_i$$
 [15]

Where x represents the grasshopper's position (feature selection variables),  $S_i$  represents the grasshoppers' social behavior (target location), G represents the grasshopper's gravitational force (moving to the best place), and A indicates the wind pattern. The final three show the grasshopper's position. To generate random behavior, the Equation (16) is used, which allows r to oscillate arbitrarily between 0 and 1:

$$X_i = r_1 S_i + r_2 G_i + r_3 A_i$$
 [16]

Equation (17) estimates the rate of social contact, which equals  $S_i$  (the target function), and  $d_{ij}$  represents the distance between the i<sup>th</sup> and j<sup>th</sup> grasshoppers.

$$S_{i} = \sum_{i=1}^{N} |||| s(d_{ii}) \widehat{d_{ii}}|$$
 [17]

Equation (18) produces the function s, which represents the distance between the grasshoppers.

$$s(r) = fe^{\frac{-r}{l}} - e^{-r}$$
 [18]

Equation (19) is the generic formula for this equation, which employs f (the ideal goal function) to represent gravitational intensity and l (the length of the gravity scale).

$$X_i = \sum_{j=1}^{N} |||| S(|X_j - X_i|) \frac{X_j - X_i}{d_{ii}} - g\widehat{e_g} + u\widehat{e_w} [19]$$

N (other features) indicates the number of grasshoppers. The modified correlation is chosen because ground-dwelling insects, and grasshoppers' locations should not exceed a particular limit. This equation determines a grasshopper's updated position using its target location, present position, and the positions of the other grasshoppers. The C, a decreasing factor influencing the repulsion, comfort, and attraction regions, is an important parameter in the GOA. Equation (20) is utilized to determine the updated parameter.

$$c = c_{max} - l \frac{c_{max} - c_{min}}{L}$$
 [20]

The most extreme values are represented by  $c_{max}$  and  $c_{min}$  in Equation (20), where l is the current iteration and L is the maximum iteration. The suggested model evaluated  $c_{max}$  at 1

and  $c_{min}$  at 0.00004. The intention behind employing the GOA for feature selection was to improve the criterion's accuracy.

### F. Naïve Bayes Classifier

The Bayesian theorem [22] is the basis of statistical and probability theory. For random variables, it reveals a connection between marginal probabilities and conditional probabilities. Let P(A) and P(B) be the prior probability representing the initial degree of belief in A, and B. Taking B into consideration increases the conditional probability to P(A|B), which is the degree of belief in A. The mathematical statement of the Bayesian theorem is given in Equation (21):

$$P(A|B) = \frac{P(B|A) P(A)}{P(B)}$$
[21]

The NB Classifier is a fundamental probabilistic classifier in AI, based on Bayes' theorem [23]. Assume D is a database training set. Each database is represented by an n-D attribute vector of n dimensions. X has n unique qualities, indicated by  $(x_1, x_2, \ldots, x_n)$ . The purpose of classification is to determine the highest  $P(C_i|X)$  exists from a set of m classes  $C_1, C_2, \ldots, C_m$ . This results from the application of Bayes' theorem.

$$P(X) = \frac{P(X|C_i)P(C_i)}{P(X)}$$
 [22]

Since P(X) is of equal value for every class, maximizing P(X) is necessary.

$$P(X) = P(X|C_i)P(C_i)$$
 [23]

Assumption number one in NB is that all qualities are conditionally independent, meaning they do not depend on each other [24]. Based on Equation (24), the test samples are assigned to their respective classes.

$$P(X|C_i) = \prod_{k=1}^{n} \mathbb{E} P(X_k|C_i) \operatorname{argmax} \{P(X|C_i)P(C_i)\} [24]$$

For instance, by the NB rule, a new sample is considered to be of class  $C_2$  if, upon its arrival, the posterior probability  $P(C_2|X)$  is the highest of all the  $P(C_k|X)$  values for all k classes.

### 3. Result and Discussion

In this section, the experimental set-up and outcomes obtained in the research on automated pneumonia detection are discussed.

### A. Experimental Set-up

The Jupyter Notebook platform was chosen to implement the experiment. The PC configuration used in the research includes a 13th-generation Intel Core i5 processor, 8 GB DDR4 RAM, 512 GB SSD Solid State Drive, and a 64-bit operating system. The programming was done in Python. The CXR data from the Mendeley site [25] was used. The collected data includes 234 normal CXR, 221 COVID-19, and 148 pneumonia CXR images. The research requires only pneumonia and normal CXR, so the COVID-19 CXR images are dropped. The images are of various dimensions, so resized them to 224x224. Next, a median filter was employed to eliminate the noise from the images. The data is highly imbalanced. Using *Nanotechnology Perceptions* Vol. 20 No. S13 (2024)

augmentation methods, the number of normal and pneumonia CXR images is increased from 234 and 148 to 300 samples each. Next, split the data into training and test sets. The training set is composed of 240 samples in each category, and the test set is composed of 60 samples. The details of the data distribution of the CXR images are given in Figure 1.

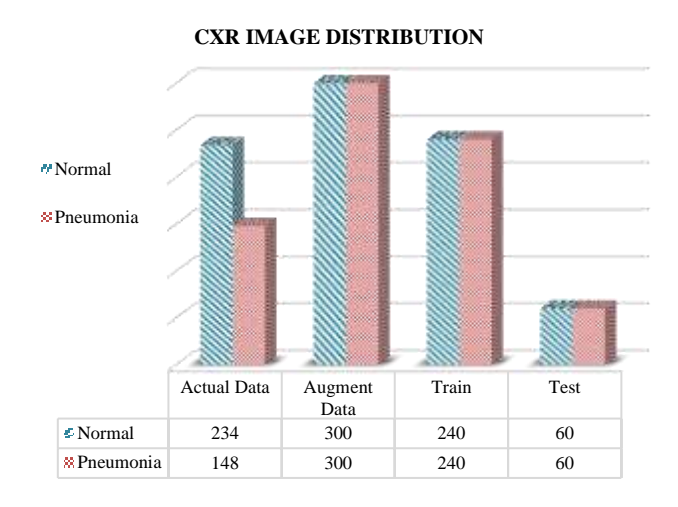


Fig. 1. Distribution of CXR images.

### B. Discussion

The processed and balanced data is given to advanced algorithms like HOG, GLCM, and LBP for feature extraction. Then, all three features are combined using the addition fusion method. Next, GOA is employed to identify the most important features from the fused features. All selected features are given to the NB model for pneumonia detection. The outcome of the NB model is evaluated using metrics such as accuracy, specificity, sensitivity, precision, F1 score, FRR, and FAR. The metrics are calculated using the confusion matrix obtained by the model. Table I gives the confusion matrix of the NB model on each feature set. In the table, TP, TN, FP, and FN represent true positive, true negative, false positive, and false negative, respectively. The TP and TN are the outcomes of correctly identified pneumonia and normal CXR images, while FP and FN are the outcomes of wrongly identified pneumonia and normal CXR images.

TABLE I. CONFUSION MATRIX OF NB MODEL USING VARIOUS FEATURES

Features	TP	TN	FP	FN
HOG	53	55	5	7
GLCM	55	56	3	6
LBP	51	54	8	7
Fused	57	58	2	3
Optimized	58	60	1	1

The calculated metrics of the NB model using the confusion matrix elements are given in Table II. The highest accuracy, specificity, sensitivity, precision, and F1 score is attained by NB when using the optimized features as input. The attained values are 98.33%, 98.36%, 98.31%, 98.31%, and 98.31%, respectively. The next highest values result from using fused features,

with resultant metrics values of 95.83%, 96.67%, 95%, 96.61%, and 95.8%. The lowest metrics values of 87.5%, 87.1%, 87.93%, 86.44%, and 87.18% are obtained when using LBP features. The comparison of NB model positive metrics outcomes when using various features is given in Figure 2.

TABLE II. COMPARISON OF NB MODEL PERFORMANCE USING DIFFERENT FEATURES

Features	HOG	GLCM	LBP	Fused	Optimized		
ACCURACY	90	92.5	87.5	95.83	98.33		
SPECIFICITY	91.67	94.92	87.1	96.67	98.36		
SENSITIVITY	88.33	90.16	87.93	95	98.31		
PRECISION	91.38	94.83	86.44	96.61	98.31		
F1	89.83	92.44	87.18	95.8	98.31		
FRR	11.67	9.84	12.07	5	1.69		
FAR	8.33	5.08	12.9	3.33	1.64		

# EVALUATION OF MLP'S POSITIVE METRICS ON VARIOUS FEATURES WHO WELLOW WELLOW WELLOW WELLOW WITH WARRY W

Fig. 2. Comparison of the NB model's positive metrics with various input features.

Next, the negative metrics FAR and FRR are evaluated. The NB model gives 11.67% and 8.33% on HOG features, 9.84% and 5.08% on GLCM features, 12.07% and 12.9% on LBP features, 5% and 3.33% on fused features, and 1.69% and 1.64% on optimized features. The negative metrics are very low when using optimized features. Figure 3 gives the comparison of negative metrics attained by the NB model on various features.

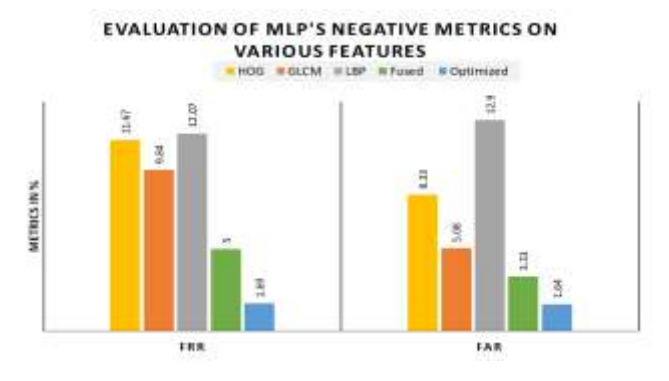


Fig. 3. Comparison of the NB model's negative metrics with various input features.

### 4. CONCLUSION

Pneumonia is a significant cause of death. According to the World Health Organization, pneumonia can be effectively treated with early detection and simple treatments. However, radiological diagnostics are lacking for the vast majority of people. While imaging technology is available, there is a shortage of X-ray experts. This paper proposes the automatic detection of pneumonia in chest X-ray images using optimized feature selection and AI techniques. The CXR images are collected from publicly accessible sites. The collected images suffer from irregular dimensions, imbalances, and noise. Pre-processing is performed to improve data quality. Features from the images are extracted using HOG, LBP, and GLCM techniques. The extracted features are then fused, and the most important features are selected using GOA. The Naive Bayes (NB) model is employed to detect pneumonia using the extracted, fused, and optimized features. The optimized features with NB yield excellent results. The proposed GOA-NB method achieved an accuracy of 98.33%, specificity of 98.36%, sensitivity of 98.31%, precision of 98.31%, F1 score of 98.31%, FRR of 1.69%, and FAR of 1.64%. In this study, we focused on determining whether a person had pneumonia. In the future, we plan to investigate more accurate optimization and AI techniques for diagnosing various forms of pneumonia, such as viral and bacterial infections.

### References

- 1. Miyashita, Naoyuki. "Atypical pneumonia: Pathophysiology, diagnosis, and treatment." Respiratory investigation 60, no. 1 (2022): 56-67.
- 2. Ticona, Javier H., Victoria M. Zaccone, and Isabel M. McFarlane. "Community-acquired pneumonia: A focused review." Am J Med Case Rep 9, no. 1 (2021): 45-52.
- 3. Ayan, Enes, and Halil Murat Ünver. "Diagnosis of pneumonia from chest X-ray images using deep learning." In 2019 Scientific meeting on electrical-electronics & biomedical engineering and computer science (EBBT), pp. 1-5. Ieee, 2019.
- 4. Li, Yuanyuan, Zhenyan Zhang, Cong Dai, Qiang Dong, and Samireh Badrigilan. "Accuracy of deep learning for automated detection of pneumonia using chest X-Ray images: A systematic review and meta-analysis." Computers in Biology and Medicine 123 (2020): 103898.
- 5. Ortiz-Toro, César, Angel Garcia-Pedrero, Mario Lillo-Saavedra, and Consuelo Gonzalo-Martin. "Automatic detection of pneumonia in chest X-ray images using textural features." Computers in biology and medicine 145 (2022): 105466.
- 6. Constantinou, Marios, Themis Exarchos, Aristidis G. Vrahatis, and Panagiotis Vlamos. "COVID-19 classification on chest X-ray images using deep learning methods." International Journal of Environmental Research and Public Health 20, no. 3 (2023): 2035.
- 7. Duong, Linh T., Phuong T. Nguyen, Ludovico Iovino, and Michele Flammini. "Automatic detection of Covid-19 from chest X-ray and lung computed tomography images using deep neural networks and transfer learning." Applied Soft Computing 132 (2023): 109851.
- 8. Singh, Sukhendra, Manoj Kumar, Abhay Kumar, Birendra Kumar Verma, Kumar Abhishek, and Shitharth Selvarajan. "Efficient pneumonia detection using Vision Transformers on chest X-rays." Scientific Reports 14, no. 1 (2024): 2487.
- 9. Athar, Atifa, Rizwana Naz Asif, Muhamamd Saleem, Sundus Munir, Mohammad Rustom Al Nasar, and Alaa M. Momani. "Improving pneumonia detection in chest X-rays using transfer learning approach (AlexNet) and adversarial training." In 2023 International Conference on

- Business Analytics for Technology and Security (ICBATS), pp. 1-7. IEEE, 2023.
- Lafraxo, Samira, Mohamed El Ansari, and Lahcen Koutti. "A new hybrid approach for pneumonia detection using chest X-rays based on ACNN-LSTM and attention mechanism." Multimedia Tools and Applications (2024): 1-23.
- 11. Shakeel, Memoona, Ahmad Naeem, Naeem Aslam, Kamran Abid, and Muhammad Qasim Shafiq. "Pneumonia Recognition in Chest X-rays through Convolutional Neural Networks (CNN)." Journal of Computing & Biomedical Informatics (2024).
- 12. Shyla, NS Jeya, and WR Sam Emmanuel. "Automated classification of glaucoma using DWT and HOG features with extreme learning machine." In 2021 Third international conference on intelligent communication technologies and virtual mobile networks (ICICV), pp. 725-730. IEEE, 2021.
- 13. Zhou, Wei, Shengyu Gao, Ling Zhang, and Xin Lou. "Histogram of oriented gradients feature extraction from raw bayer pattern images." IEEE Transactions on Circuits and Systems II: Express Briefs 67, no. 5 (2020): 946-950.
- 14. Haralick, Robert M., Karthikeyan Shanmugam, and Its' Hak Dinstein. "Textural features for image classification." IEEE Transactions on systems, man, and cybernetics 6 (1973): 610-621.
- 15. Mohanaiah, P., P. Sathyanarayana, and L. GuruKumar. "Image texture feature extraction using GLCM approach." International journal of scientific and research publications 3, no. 5 (2013): 1-5.
- 16. Ojala, Timo, Matti Pietikainen, and Topi Maenpaa. "Multiresolution gray-scale and rotation invariant texture classification with local binary patterns." IEEE Transactions on pattern analysis and machine intelligence 24, no. 7 (2002): 971-987.
- 17. Pietikäinen, Matti, Abdenour Hadid, Guoying Zhao, and Timo Ahonen. Computer vision using local binary patterns. Vol. 40. Springer Science & Business Media, 2011.
- 18. Guo, Zhenhua, Lei Zhang, and David Zhang. "A completed modeling of local binary pattern operator for texture classification." IEEE transactions on image processing 19, no. 6 (2010): 1657-1663.
- 19. Boulahia, Said Yacine, Abdenour Amamra, Mohamed Ridha Madi, and Said Daikh. "Early, intermediate and late fusion strategies for robust deep learning-based multimodal action recognition." Machine Vision and Applications 32, no. 6 (2021): 121.
- 20. Zakeri, Arezoo, and Alireza Hokmabadi. "Efficient feature selection method using real-valued grasshopper optimization algorithm." Expert Systems with Applications 119 (2019): 61-72.
- 21. Alirezapour, Hanie, Najme Mansouri, and Behnam Mohammad Hasani Zade. "A Comprehensive Survey on Feature Selection with Grasshopper Optimization Algorithm." Neural Processing Letters 56, no. 1 (2024): 28.
- 22. Hanson, Robin, John Stutz, and Peter Cheeseman. Bayesian classification theory. No. NAS 1.15: 107885. 1991.
- 23. Rish, Irina. "An empirical study of the naive Bayes classifier." In IJCAI 2001 workshop on empirical methods in artificial intelligence, vol. 3, no. 22, pp. 41-46, 2001.
- 24. Yang, Feng-Jen. "An implementation of naive bayes classifier." In 2018 International conference on computational science and computational intelligence (CSCI), pp. 301-306. IEEE, 2018.
- 25. Shams, Mahmoud, Omar Elzeki, Mohamed Abd Elfattah, and A. Hassanien. "Chest X-ray images with three classes: COVID-19, Normal, and Pneumonia." Mendeley Data 3 (2020).